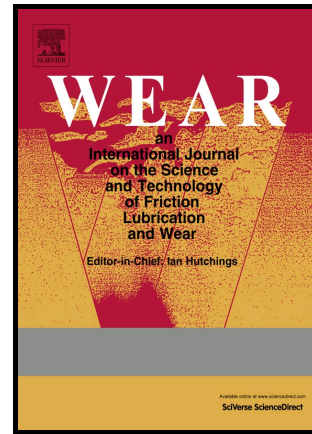


## Author's Accepted Manuscript

### ON THE INFLUENCE OF CAR BRAKE SYSTEM PARAMETERS ON PARTICULATE MATTER EMISSIONS

Mattia Alemani, Jens Wahlström, Ulf Olofsson



[www.elsevier.com/locate/wear](http://www.elsevier.com/locate/wear)

PII: S0043-1648(17)30995-X  
DOI: <https://doi.org/10.1016/j.wear.2017.11.011>  
Reference: WEA102293

To appear in: *Wear*

Received date: 14 July 2017  
Revised date: 14 November 2017  
Accepted date: 15 November 2017

Cite this article as: Mattia Alemani, Jens Wahlström and Ulf Olofsson, ON THE INFLUENCE OF CAR BRAKE SYSTEM PARAMETERS ON PARTICULATE MATTER EMISSIONS, *Wear*, <https://doi.org/10.1016/j.wear.2017.11.011>

This is a PDF file of an unedited manuscript that has been accepted for publication. As a service to our customers we are providing this early version of the manuscript. The manuscript will undergo copyediting, typesetting, and review of the resulting galley proof before it is published in its final citable form. Please note that during the production process errors may be discovered which could affect the content, and all legal disclaimers that apply to the journal pertain.

# ON THE INFLUENCE OF CAR BRAKE SYSTEM PARAMETERS ON PARTICULATE MATTER EMISSIONS

Mattia Alemani<sup>a,b</sup>, Jens Wahlström<sup>b</sup>, Ulf Olofsson<sup>b</sup>

<sup>a</sup>Brembo Freni S.p.A, Viale Europa 2, 24040 - Stezzano (BG), Italy

<sup>b</sup>KTH Royal Institute of Technology, Stockholm, Sweden

December 2016

Corresponding Author: Mattia Alemani

mattia\_alemani@brembo.it

## ABSTRACT

The influence of car brake system parameters on particulate matter emissions was investigated using a pin-on-disc tribometer. Samples from a low-steel friction material and a cast iron disc were tested for different sliding velocities, nominal contact pressures and frictional powers. Disc temperatures were also measured. Their impact on total concentration, size distribution, particle coefficient and transition temperature was analysed. Results show that frictional power is the most significant brake system parameter. However, temperature, as a response parameter, is the most influential, inducing a shift towards the ultrafine particulate fraction and raising emissions. A transition temperature, independent of the system parameters, was identified.

**Keywords:** Brake environmental design, Frictional heating, Particulate Matter, Particle Coefficient

## 1. INTRODUCTION

Among road-traffic related pollutants, brakes have been estimated to contribute 55% by weight to the total non-exhaust PM<sub>10</sub> emissions fraction (i.e. airborne particles with an aerodynamic diameter of less than 10 µm). Furthermore, they account for 21% of overall road-traffic related PM<sub>10</sub> emissions [1]. In addition, particulate matter (PM) induces adverse health effects [2,3] and contributes to climate change. Previous studies also show existing relations with cardiovascular and respiratory diseases [4,5] and also classify this pollutant as carcinogenic [6]. Moreover, PM's black-carbon content boosts global warming whereas other elements such as, e.g. organic carbon, may have a cooling effect [7].

So far, most of the scientific publications in the disc brake aerosol research community have focused on emissions characterization; that in order to better assess how particles can interact with human beings and the environment. Hence, a wide variety of studies, performed at different test scales, is available: real scale (field tests) [8,9], system scale (dynamic bench tests) [10–12] and model scale (pin-on-disc tribometers) [13–15], among which promising correlations have also been found [16,17]. These scientific studies provide a qualitative description of particle emission in terms of size distribution, emission factors, chemical composition and particle morphology. However, they do not explain how the brake system parameters affect the generation of PM. Nevertheless, some interesting observations are provided. Kukutschová et al. [10] noticed an increase in particle number concentration in the ultrafine fraction when the rotor temperature exceeded 300°C. Garg. et al. [11] also noticed a

mass reduction in the airborne fraction and an increase in particle number for temperatures close to 400°C. Similarly, Wahlström et al. [18] found that the ultrafine number concentration in a pin-on-disc tribometer set-up increases by several magnitude orders for high load tests, i.e. the one with the highest disc temperature.

Few studies have tried to further investigate the causes of origin of particulate matter. Eriksson et al. have introduced the contact plateau models [19]. These plateaus were also observed by Österle et al. [20], while investigating tribofilm generation. Nevertheless, these studies focus on a mesoscopic scale to explain wear and friction mechanisms.

In order to include particles emissions in brake system design and simulation routines [21], a clear and complete understanding of their causes of origin, on a macroscopic scale, is still missing.

The aim of this study is to investigate how airborne PM emissions are influenced by typical car brake system parameters and map their relations. In particular, the following will be investigated: speed ( $v$ ), contact pressure ( $p$ ) and braking power ( $P$ ). Temperature ( $T$ ) will also be analysed as a significant response parameter, resulting from the developed braking power and the system cooling conditions. Speed and pressure can be classified as control parameters since they are governed by the driver; braking power is a derivative parameter since it depends on the control parameters and the coefficient of friction.

## 2. METHOD

### 2.1 Experimental set-up

All tests were performed on a model-scale, making use of a pin-on-disc tribometer with a horizontal rotating disc and a dead weight loaded pin, enclosed in a sealed chamber. This system, previously described by Olofsson et al. [22], has specifically been designed for airborne particles measurements. While such set-up substantially differ from a real vehicle set-up for, e.g., the contact orientation and the lack of dynamics, which should be considered for future studies, is nowadays difficult to measure emissions on-road due to the relevant number of emission sources [23]. In addition the need to have a simplified model of the brake contact, where a steady state can be reached, and parameters could be easily modified led to the usage of a pin on disc tribometer. Its scheme is provided in Figure 1. Ambient air (A), with a mean relative humidity of  $24 \pm 1\%$  and mean temperature of  $20.5 \pm 1.2$  °C, enters the system. The air is forced by a pump (B), set to a flow-rate of  $7.7 \text{ m}^3/\text{h}$ , through an HEPA filter (C). The latter removes particles with a collection efficiency of 99.95%, at the Maximum Penetrating Particle Size (Class H13 according to standard EN 1822). The now clean air enters the sealed test chamber (F) through the inlet (E). Here, the air-flow is continuously controlled by a hot-wire anemometer. The pin-on-disc tribometer lies inside the chamber. The approximate volumes are  $0.135 \text{ m}^3$  and  $0.035 \text{ m}^3$  respectively, giving an air-volume exchange rate of about 77 exchanges/h.

A thermal insulating ROBURIT<sup>®</sup> back-plate is fixed on the rotating base (M) and the disc sample (I) is screwed on top of that. The latter can rotate up to 3000 rpm thanks to a synchronous servo motor. Conversely, the pin (K) is mounted in a stationary pin-holder; this is fixed on an arm (G) at the end of which a dead weight (L) is positioned. The ratio between the arm hinge, the pin position, and the dead-weight is fixed, intensifying the normal force by 2.1 times (e.g. a normal force of 30N at the tip of the arm provides 63N on the pin). Differently, the tangential force is measured by a beam load cell with a nominal load of 100 N and a nominal sensitivity of 2 mV/V.

When the system is loaded and the disc is rotating, the generated airborne fraction is well mixed to the clean air volume (H). This is because of the complicated internal geometries. The air flux finally passes through the chamber outlet (J) where it is sampled.

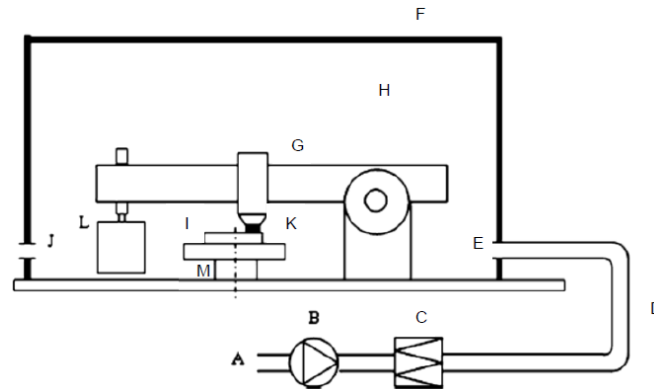


Fig.1: pin-on-disc tribometer scheme [22]. (A) Room air; (B) Fan; (C) HEPA Filter; (D) Flexible tube; (E) Clean air inlet;(F) closed box; (G) Pin-on-disc machine; (H) sampled air volume; (I) Rotating disc sample; (J) Air outlet/sampling point;(K) pin sample; (L) Dead weight; (M) rotating base;

At the outlet, particle emissions were measured using a DEKATI<sup>®</sup> ELPI+<sup>™</sup>, an Electrical Low Pressure Impactor; this both counts and collects particles on aluminium filters, in a size range of 0.0006  $\mu\text{m}$  – 10  $\mu\text{m}$ , divided into 14 different stages. The sample flow-rate is imposed at 10 L/min. The sampling rate was set at 1 Hz, a good enough frequency not to hide interesting phenomena, as shown from another study performed on a system-scale [24]. Even though pin-on-disc tests provide mainly stationary conditions, particle emissions can show dynamic behaviour depending on the system temperature; the latter was therefore measured using K-type thermocouples. Only the disc temperature was acquired, using a slippery contact. The sampling rate was set at 2 Hz.

## 2.2 Materials

Pin samples with a 10 mm diameter were machined from a real low-steel brake pad the XRF composition of which is shown in Table 1. The same pad material has previously been investigated by Alemani et al.[25] and code named M1. Equally, disc samples with a 63 mm diameter and 6 mm thick, were machined from a real disc braking surface, the chemical composition of which is shown in Table 2. Both specimens were taken from a typical European car brake system as described by Holmberg et al. [26]. This consists of a four piston monolithic calliper, two low-steel brake pads with a surface area of 77cm<sup>2</sup> and a ventilated cast iron disc. The vehicle specifications can be found in [27]. Each pin and disc sample was drilled to allow temperature measurements 3 mm below each contact surface. The disc centre to pin-centre distance was set to 25 mm, also corresponding to the disc temperature measurement point.

Table 1: Pin/pads chemical composition [wt%] obtained by XRF analysis

Mg	Si	Al	S	Ca	Fe	Cu	Zn	Cr	Zr	Sn	Ba	C
11.1	6.3	9.8	5.6	5.2	7.6	5.8	13.4	3.5	0.1	9.3	-	22.3

Table 2: Disc/rotor chemical composition [wt%] obtained by optical emission spectrometry

<b>C</b>	<b>Si</b>	<b>Mn</b>	<b>P</b>	<b>S</b>	<b>Cu</b>	<b>Cr</b>	<b>Fe</b>
3.40	1.70	0.57	0.03	0.26	0.24	0.20	93.6

### 2.3 Design of experiment

Two tests for each pressure-velocity combination, as provided in Table 3 and shown in figure 2, were performed. The run order was randomized to reduce systematic errors. The selected levels were chosen considering urban driving conditions. For the chosen vehicles, fluid pressures were in the range 18-45 bar, while vehicle speeds were between 5 km/h and 62 km/h. The same pressure levels were used by Alemani et al. [25]. In addition, the present study expands the investigation to different speed levels. Once the pin-on-disc tribometer was completely set, and the chamber cleaned and sealed, the pump was turned on. This was to flush the air volume until no particles were detected. Meanwhile, the ELPI+ was checked for leakages and zeroed. Once the latter was ready and the chamber cleanliness verified, the selected test was started. The motor was programmed to automatically stop at a sliding distance of 14148 m.

Table.3: Summary of the testing conditions for the full test plan. Conditions used for ANOVA are marked by a + or -, indicating high or low levels respectively. Subscript indexes 1 and 2 indicate to which performed ANOVA they belong (1. pressure-velocity, 2. pressure-frictional power)

<b>Test ID</b>	<b>Sliding velocity [m/s]</b>	<b>Nominal contact pressure [MPa]</b>	<b>Sliding distance [m]</b>	<b>Test time [s]</b>	<b>Frictional power [W]</b>
<b>1</b>	0.66	1.67	14148	21600	43.0
<b>2</b>	1.31 (- <sub>1</sub> )	0.55 (- <sub>1</sub> )	14148	10800	28.7
<b>3</b>	1.31 (- <sub>1</sub> )	1.11 (+ <sub>1,2</sub> )	14148	10800	57.3 ( <sub>2</sub> )
<b>4</b>	1.31	1.67	14148	10800	86.0
<b>5</b>	1.97 (+ <sub>1</sub> )	1.11 (+ <sub>1,2</sub> )	14148	7200	86.0 (+ <sub>2</sub> )
<b>6</b>	1.97 (+ <sub>1</sub> )	0.55 (- <sub>1</sub> )	14148	7200	43.4
<b>7</b>	2.62	0.55(- <sub>2</sub> )	14148	5400	57.8 (- <sub>2</sub> )
<b>8</b>	3.92	0.55 (- <sub>2</sub> )	14148	3598	86.7 (+ <sub>2</sub> )
<b>9</b>	7.86	0.13	14148	1800	43.0

The obtained data were then analysed in terms of mean total number concentration and mean specific particle coefficient. The former is defined as the sum of all the measured stage concentrations [# /cm<sup>3</sup>] for each given sample. Therefore, the total number concentration is the one of particles ranging from 0.006 to 10 µm. Note that the particle coefficient will be defined in Section 3: Theory.

In addition, the mean number size distribution [# /cm<sup>3</sup>] was considered. This is defined as the measured concentration by each single stage. However, this was normalized by the stage characteristic diameter. This is done to allow future comparison with different particle measurement instruments.

All the quantities were calculated as mean values for steady-state conditions of the system temperature; that is, taking only into consideration measured values for disc temperatures exceeding 90% of the maximum recorded one. The influence of pressure and velocity, as well as their interaction (i.e. frictional power) was investigated performing a two-way ANOVA [28], using two repetitions. The selected levels were 0.55 MPa and 1.67 MPa for the pressure, and 1.31 and 1.96 m/s for the sliding

velocity. Similarly, a comparison between pressure and frictional power was performed. The selected levels were 0.55 and 1.11MPa, and 57 and 86W, respectively. These levels are highlighted in Table 3 by a “+”, for the high one, or by a ‘-‘for the low one. Subscripts ‘1’ or ‘2’, indicate the performed ANOVA in the presented order.

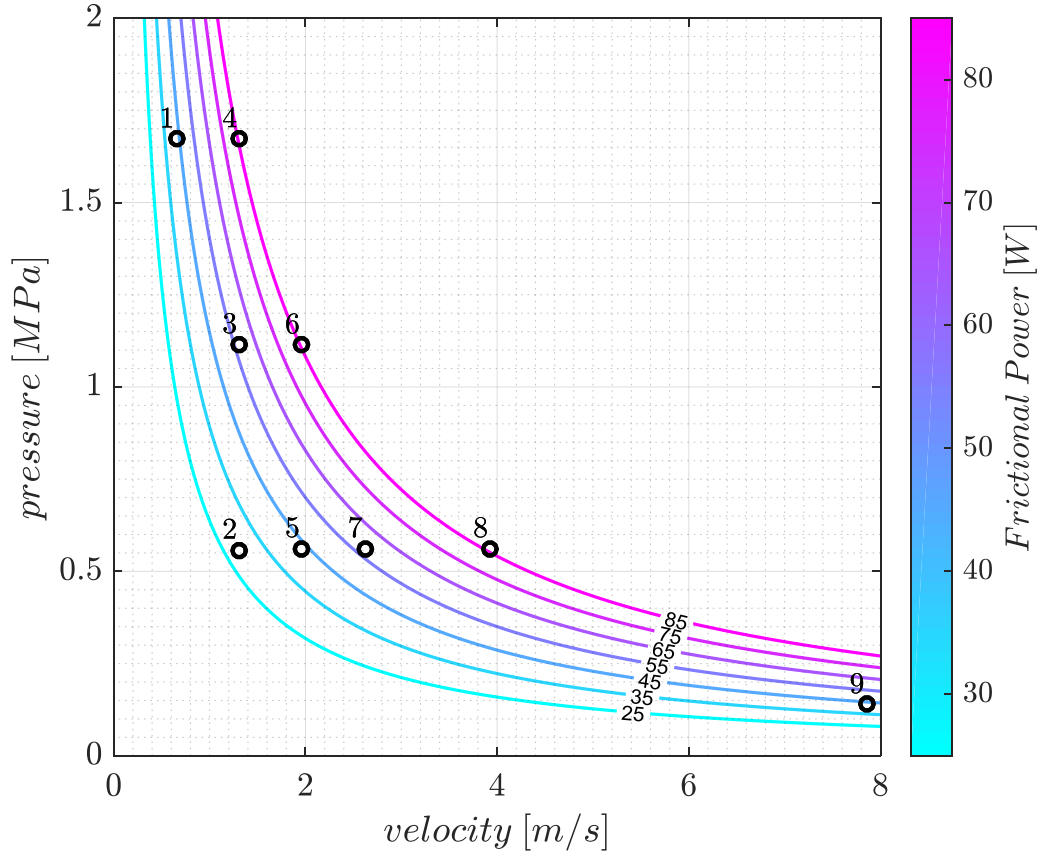


Figure 2: Pressure-velocity conditions map. Iso-Frictional Power line are visible, showing which of the tests had a similar power. The investigated conditions are shown by black dots.

### 3. THEORY

A brake system is designed to transform the vehicle kinetic energy into heat, aiming for full stops or a speed reduction, in a desired space. This energy transformation results in a variable increase in system temperature per cooling condition (i.e. rotor design, air temperature, rim design, etc.) and developed frictional power.

The latter is dependent on three typical brake system parameters: the friction coefficient, the normal force, and the sliding velocity. This relation is presented in Eq.(1):

$$P = \mu N v \quad \text{Eq.(1)}$$

where P is the frictional power,  $\mu$  is the friction coefficient, N is the normal load, and v is the sliding velocity. These parameters, on a real brake system, result from the vehicle speed, the applied brake pressure and the pads' friction material respectively. Almost all of them have been investigated in previous studies. Indeed, the relation between emissions and nominal contact pressure, i.e. brake

pressure, has been explored [18,29], showing a general increase in emissions with rising contact pressures. However, such an increase seems to be non-linear and mainly caused by the ultrafine fraction. Different friction coefficients [9,11,25], i.e. different friction materials, were also studied. The results show lower emissions for NAO materials and still a non-linear relationship against the load, irrespective of the analysed material. In contrast, the influence of the sliding velocity has not been deeply investigated yet.

Recent studies [30] also reveal that there are two temperature levels affecting the total particle number concentration. The first temperature range, identified between 40°C-95°C, affects the fine fraction; the second one, between 165°C-190°C, affects the ultrafine fraction. It has also been verified that this phenomenon occurs for different friction materials irrespective of their chemical composition, i.e. Low-Steel, Very-Low-Steel or Non-Asbestos Organic (NAO).

This emissions temperature dependence, if confirmed, should be then considered in simulations. This can be done by making use of emission factors. The literature proposes different ways of calculating it, using particle mass or number. Among the latter, the most common are particle number per stop [11], per unit sliding distance [22], per unit time [15] or per unit friction energy [30]; among the former, particle mass per stop [9] or per sliding distance [31] are widespread. However, Olofsson et al. [32] took a further step forward by calculating the particle coefficient ( $k_{air}$ ). This is an extension of the Archard-Holm's wear coefficient [33] and can be interpreted as the probability a wear particle is generated and becomes airborne:

$$\frac{N_{air}}{S} = k_{air} \frac{4W}{H\pi D_i^3} \quad \text{Eq.(2)}$$

where  $N_{air}/S$  is the emission factor expressed as particle number per slid distance  $S$ ,  $W$  is the normal force,  $H$  is the material hardness and  $D_i$  is the wear particle diameter, assuming that particles are spherical.

Wahlström et al. [34] proposed a simulation methodology based on pin-on-disc tests for  $k_{air}$  calculation using a low steel pad material against a cast iron disc. This methodology showed promising results for steady state running conditions, along with the need to create an emission map covering a wider operational range. Note that the characterization of pad hardness can be difficult since such a component is very heterogeneous and made of different materials ranging from polymers to steels.

Therefore, rewriting Eq. 2, this paper will propose a particle coefficient,  $k'_{air}$  [# /MPa], which is specific to the frictional couple hardness ( $k_{air} / H$ ). This implies that the obtained results will be valid only for the analysed frictional couple, whose chemical compositions are stated in Tables 1 and 2. Adding a direct dependence on the pressure, instead of the normal load ( $W$ ), the specific particle coefficient can be calculated as in Eq.(3)

$$k'_{air} = \frac{N_{air}}{S} \frac{\pi D_i^3}{4pA} \quad \text{Eq.(3)}$$

where  $p$  is the nominal contact pressure, and  $A$  is the nominal contact area.

In addition, to help simplify the simulation routines, a specific  $k'_{air}$  for each size fraction - i.e. ultrafine (UF), fine (F) and coarse (C) - is given. Such reduction of available coefficients is meant to provide the minimum amount of data while keeping information on the aforementioned commonly recognized size fractions. Indeed, it should be considered that a set of  $k'_{airFRACTION}$  should be available for any brake parameters combination, therefore a reduction in particle coefficients would be beneficial for

calculations speed. The  $k'_{airFRACTION}$  coefficient, in this papers, is calculated as a weighted mean of the different coefficients belonging to the considered size fraction, weighted for the mean particle diameter,  $D_i$ , provided by the measurement instrument, as in Eq.(4).

$$k'_{airFRACTION} = \frac{\sum_{i=l\ min}^{l\ max} k'_{air,i} D_i}{\sum_{i=1}^n D_i} \quad \text{Eq.(4)}$$

Note that in this study the size fraction are defined according to the particles aerodynamic diameters ( $d_a$ ) as follow: coarse fraction for  $10\ \mu\text{m} < d_a \leq 2.5\ \mu\text{m}$  ; fine fraction for  $2.5\ \mu\text{m} < d_a \leq 0.1\ \mu\text{m}$ ; and ultrafine fraction for  $d_a < 0.1\ \mu\text{m}$ .

Each of the aforementioned  $k'_{airFRACTION}$  coefficients will then need a single significant diameter which can be calculated as the geometrical mean between the one belonging to the considered size fraction, as in Eq.(5):

$$D_{FRACTION} = \sqrt[l]{\prod_{i=l\ min}^{l\ max} D_i} \quad \text{Eq.(5)}$$

While Eq.3-5 provides a specific particle coefficient for each size fraction, which can be useful for an estimation of a frictional couple overall emissions under simulation routines as from [34], it has to be underlined that no relations to the basic particle generation phenomena, such as nucleation processes, are provided.

## 4. RESULTS

Table 4 shows the mean total number concentration and mean specific particle coefficient for each size range ( $k'_{airFRACTION}$ ), i.e. coarse, fine and ultrafine. Both parameter results are calculated as the mean of the two performed repetitions and refer to steady-state conditions, for the system temperature, as stated in Section 2.3. Note that used values are as measured, therefore particle coefficients equal to 0 can occur, meaning that no particles were registered in that specific size range. According to Eq.(5), the size fraction diameters to be considered for the particle coefficients are  $D_{COARSE} = 6.9\ \mu\text{m}$ ,

$$D_{FINE} = 0.12\ \mu\text{m} \text{ and } D_{ULTRAFINE} = 0.0012\ \mu\text{m}.$$

Table 4: Testing conditions mean total number concentrations and specific particle coefficient values. Results are calculated as the mean of the two performed repetitions.

Test ID	Sliding velocity [m/s]	Nominal contact pressure [MPa]	Mean total number concentration [# / cm <sup>3</sup> ]	Specific Particle Coefficient [# / MPa]		
				Coarse	Fine	Ultrafine
1	0.66	1.67	2.93 10 <sup>6</sup>	2.70 10 <sup>-7</sup>	0.00	2.74 10 <sup>-5</sup>
2	1.31	0.55	1.14 10 <sup>3</sup>	2.06 10 <sup>-3</sup>	2.59 10 <sup>-4</sup>	2.40 10 <sup>-7</sup>
3	1.31	1.11	2.66 10 <sup>6</sup>	4.19 10 <sup>-5</sup>	2.70 10 <sup>-7</sup>	3.95 10 <sup>-5</sup>
4	1.31	1.67	8.36 10 <sup>6</sup>	3.59 10 <sup>-4</sup>	4.87 10 <sup>-5</sup>	2.23 10 <sup>-4</sup>
5	1.97	0.55	8.56 10 <sup>2</sup>	3.66 10 <sup>-3</sup>	3.19 10 <sup>-4</sup>	2.30 10 <sup>-7</sup>
6	1.97	1.11	1.07 10 <sup>7</sup>	6.45 10 <sup>-5</sup>	3.50 10 <sup>-7</sup>	1.09 10 <sup>-4</sup>
7	2.62	0.55	1.15 10 <sup>5</sup>	4.30 10 <sup>-3</sup>	4.29 10 <sup>-4</sup>	5.20 10 <sup>-7</sup>
8	3.92	0.55	9.00 10 <sup>6</sup>	0.00	0.00	3.30 10 <sup>-5</sup>

Figure 3 shows a pressure – velocity map for the total number concentration (see Table 4). In addition, a linear interpolation of the obtained values has been performed to forecast the unexplored parameter combinations. It is possible to observe how, moving to the up-right (increasing power), emissions reach a peak from where they start to decrease.

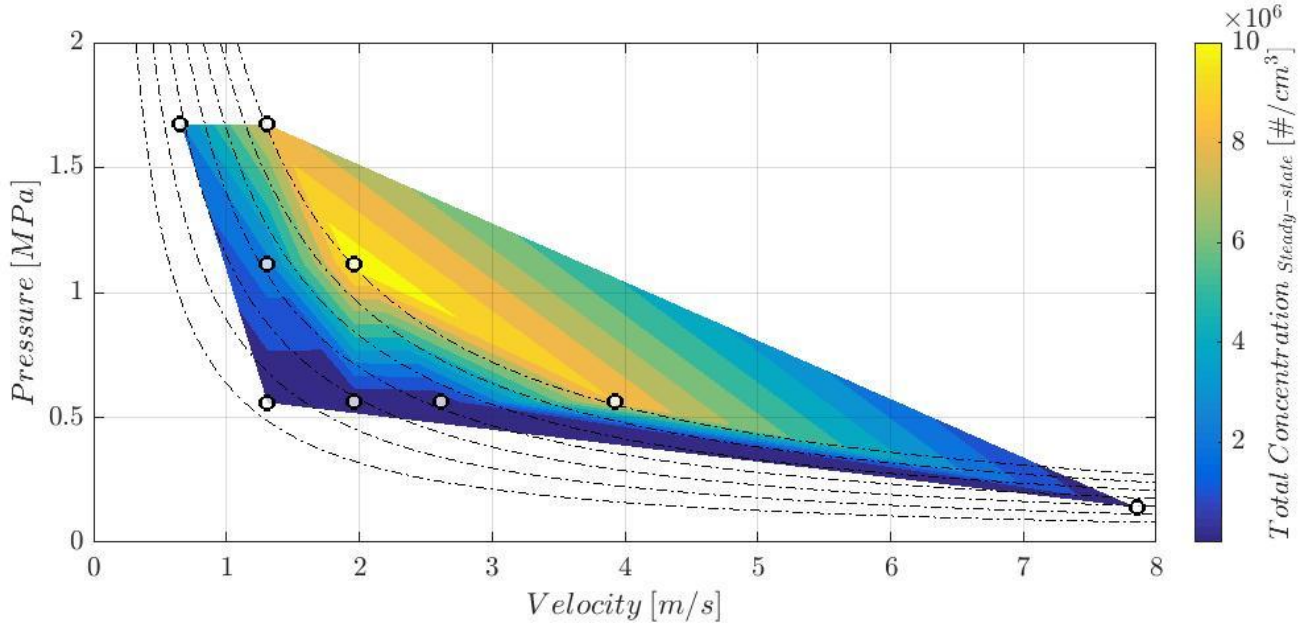


Figure 3: pressure-velocity-total concentration map. The plot shows the emissions intensity, in terms of mean total number concentration for each pressure-velocity combination tested, during the steady state. An emissions prediction for the surrounding conditions was performed.

An analysis of variance (ANOVA) for a  $2^2$  factorial design, where the considered factors are pressure and sliding velocity, is shown in Table 5. The selected high and low levels are respectively 0.55 MPa and 1.67 MPa for pressure and 1.31 and 1.97 m/s for the sliding velocity. The output is given in terms of mean total number concentration for steady-state conditions of the disc temperature.

Table 5:  $2^2$  ANOVA results for mean steady-state total number concentration. The set levels were: 0.55 MPa and 1.11 MPa as nominal contact pressure; 1.31 m/s and 1.97 m/s as sliding velocity

Source	SS	df	MS	F	Prob>F
Sliding velocity	$3.21 \cdot 10^{13}$	1	$3.21 \cdot 10^{13}$	1.31	0.32
Nominal contact pressure	$8.89 \cdot 10^{13}$	1	$8.89 \cdot 10^{13}$	3.64	0.13
Interaction	$3.21 \cdot 10^{13}$	1	$3.21 \cdot 10^{13}$	1.31	0.32
Error	$9.78 \cdot 10^{13}$	4	$2.45 \cdot 10^{13}$		
Total	$2.51 \cdot 10^{14}$	7			

Table 6 shows the ANOVA results where the considered parameters are pressure and power. The set levels were 0.55 MPa and 1.11 MPa for the former and 57 W and 86W for the latter. Power is calculated as in Eq.(1). Results are given as for the previous analysis. Even if the frictional power p-value is close to 0.1, there is a strong evidence for its importance compared to the contact pressure.

Table 6: 2<sup>2</sup> ANOVA results for mean steady-state total number concentration. The set levels were: 0.55 Mpa and 1.11 MPa as nominal contact pressure; 57W and 86W as frictional power

Source	SS	df	MS	F	Prob>F
Frictional Power	1.4310 <sup>14</sup>	1	1.4310 <sup>14</sup>	5.21	0.08
Nominal contact pressure	8.9110 <sup>12</sup>	1	8.9110 <sup>12</sup>	0.32	0.60
Interaction	3.8010 <sup>11</sup>	1	3.80 10 <sup>11</sup>	0.01	0.91
Error	1.1010 <sup>14</sup>	4	2.74 10 <sup>13</sup>		
Total	2.6210 <sup>14</sup>	7			

The performed ANOVA analysis indicates that frictional power is the most important parameter for particle emissions.

Figure 4b, 4c and 4f show the particle size distribution for each testing condition. These were calculated as the mean of the two repetitions performed. The corresponding test parameters are shown in Figures 4a, 4c and 4d. Tests are grouped by nominal contact pressure levels. Similar colours for each size distribution line indicate similar velocities. How the size distribution changes is clearly visible, showing a predominance of ultrafine fraction for all the tests lying over the 45W power level.

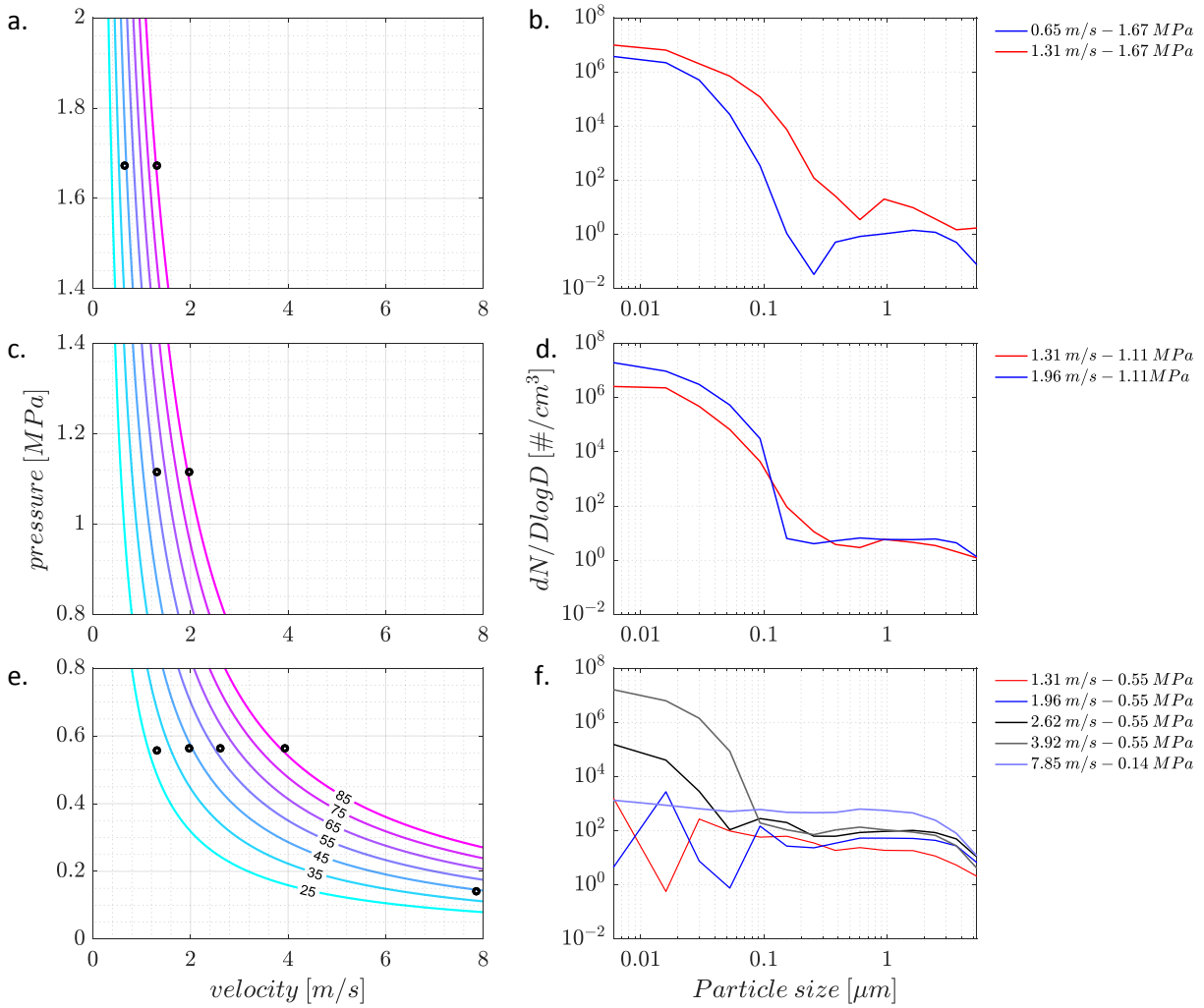


Figure 4: Mean size distributions for the different testing conditions(4b,4d,4e), along with the corresponding  $p$ - $v$ - $P$  maps and testing points (4a,4c,4e).

Figure 5 shows the total number concentration values, plotted against the disc temperature, for each test, during the steady-state. Irrespective of the working conditions, emissions show a steep increase above the temperature range 170-190°C. Results from testing conditions no. 9 (see Table 3) are not shown due to limitations in temperature measurements, given by the high rotational speed. The chosen dot colours recall power lines in Figure 2.

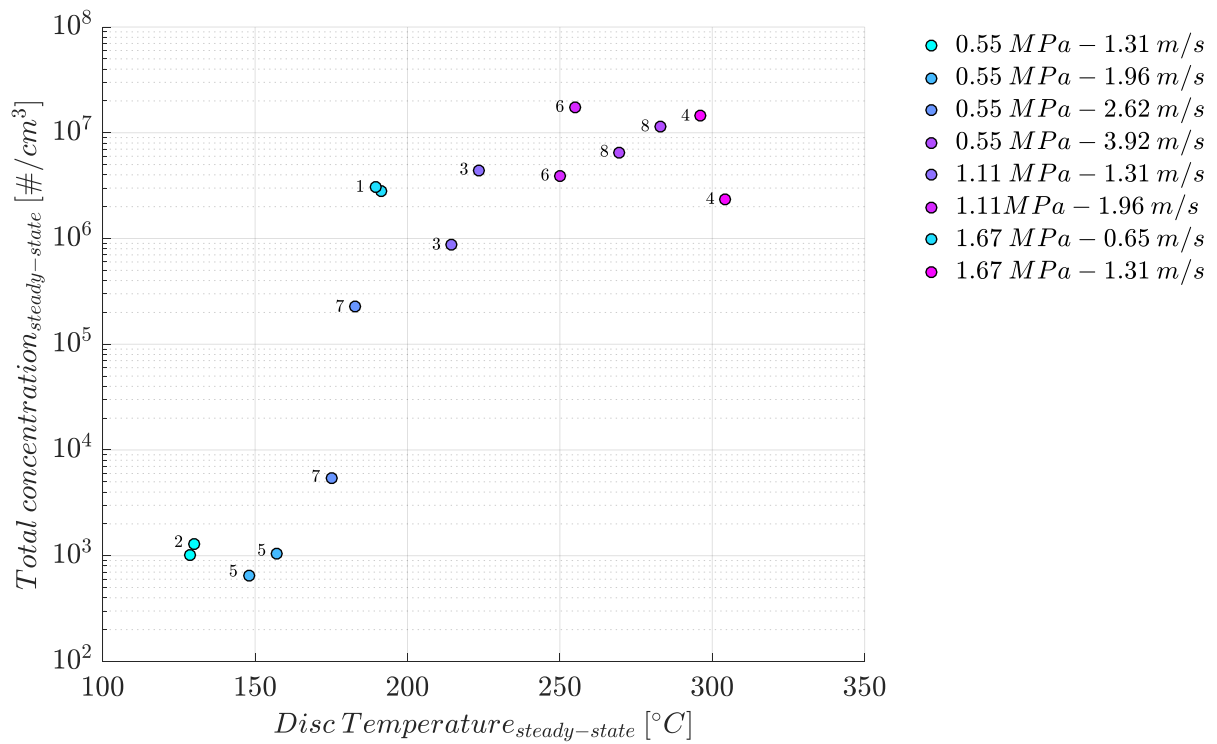


Figure 5: Steady-state number concentration against the steady-state disc temperature for the performed tests. Testing conditions no.9, as in Table 3, are not included due to acquisition system limitations.

Figure 6 shows the specific particle coefficients values for each size fraction, as provided by Table 4. Once again, a prediction of the surrounding test points was performed. A clear difference in particle generation mechanism is shown. Coarse and fine particles seems to be more sensitive to velocity whereas the ultrafine fraction is susceptible to pressure.

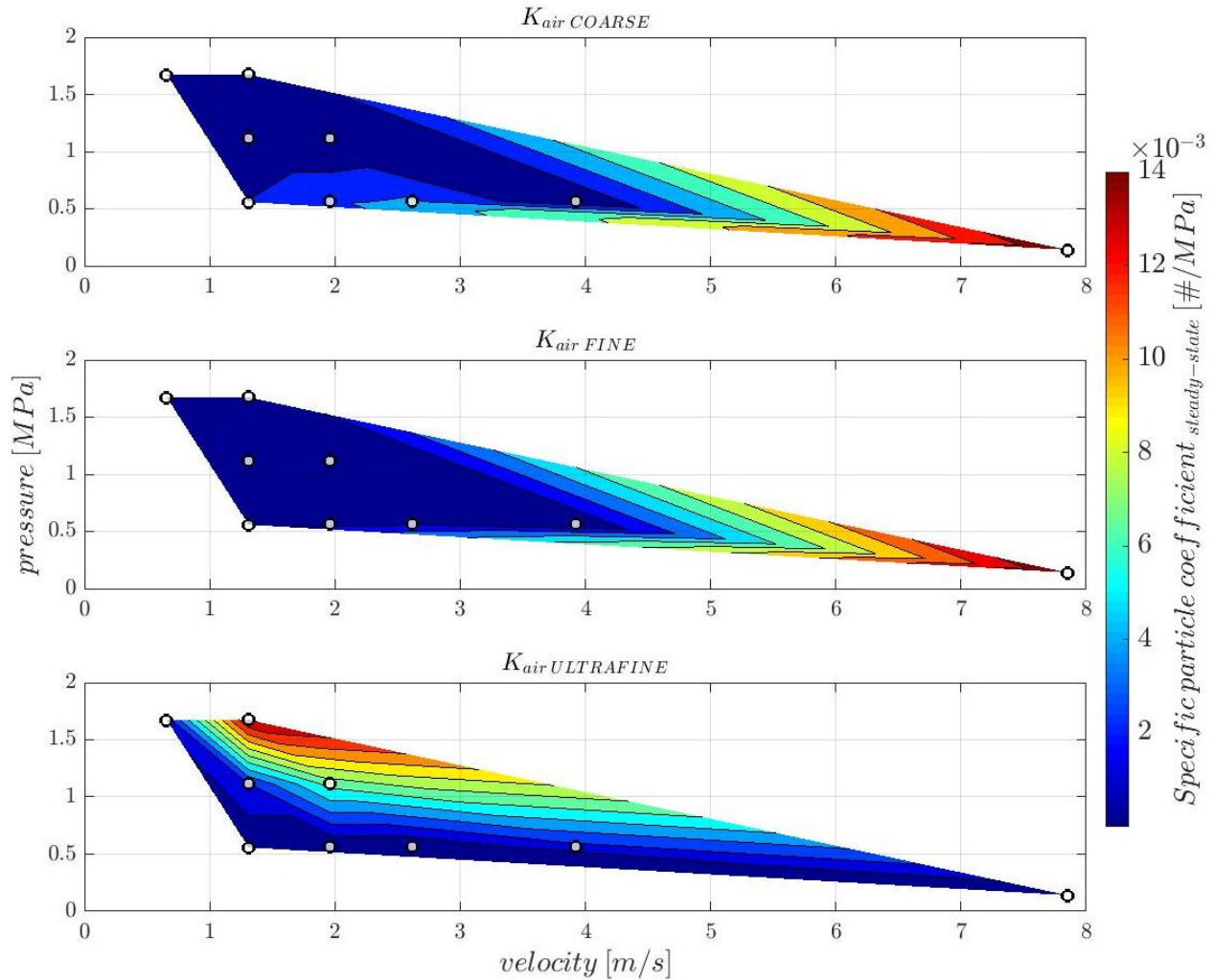


Figure 6: Pressure-velocity-specific particle coefficients ( $k'_{air}$ ) plot. The figures shows specific particle coefficients for coarse (6a), fine (6b) and ultrafine (6c) fractions, for the tested conditions. A prediction of the surrounding conditions was also performed.

## 6. DISCUSSION

The map in Figure 3 suggests that, among the considered brake system parameters (i.e. pressure, speed and frictional power), frictional power is the most influential one. Indeed, the mean steady-state total concentration increase correlates to a reasonable extent with the iso-frictional-power lines until a peak is reached, around 85W, for condition no. 5 (see Table 4). Afterwards, emissions start to decrease. This latter phenomenon is an interpolation artefact induced by the lack of measured points in that specific area. In turn, this is due to testing equipment limitations. Therefore, values over the 85W power line should not be considered as reliable.

A statistical evidence of the frictional power importance is also provided by the ANOVA results presented in Tables 5 and 6. Indeed, when comparing sliding velocity and nominal contact pressure (Table 5), the latter results as the most significant parameter, with a p-value of 0.12. Nevertheless, when comparing frictional power and nominal contact pressure (Table 6), the former is the most

significant, with a p-value of 0.08. Note that only two repetitions were performed in this study; this may explain the high p-values.

In a brake system, the controlled parameters are therefore not individually responsible for emissions. What is important is how they are combined, along with the friction coefficient, resulting in frictional power (see Eq.(1)). The higher the frictional power, the more the emitted particles. Note that the friction coefficient in this study was treated as a constant directly related to the friction material.

However, not only the overall emissions are susceptible to the brake parameters. Number size distributions also change depending on each test configuration, as shown in Figure 4. In addition, the distribution seems more sensitive to the disc temperature than to brake system parameters. Indeed, when combining the results from Figures 4 and 5, it is evident how emissions reach higher values, especially due to the ultrafine fraction, when the transition temperature [25] is reached and overcome.

Clear confirmations are provided in Figures 4b,d: all considered tests (1,4,3,6) show high emissions, with a peak in the ultrafine fraction, and high temperature values, but different frictional powers. Conversely, tests 5 and 1 (Fig 4b,f) have the same frictional power but different size distributions, depending on the disc temperature. Such results are in agreement with previous observations by Kukutschova et al. [10], Garg et al. [11] and Alemani et al. [27,29]. Therefore, it can be stated that temperature is even more important than frictional power. This observation is confirmed by Figure 5.

Indeed, the temperature increase is clearly connected to a significant increase in emissions. In addition, the latter occurs in a specific temperature range which is independent of any brake system or response parameter. In other words, Figure 5 illustrates how an increase in emissions by several magnitude order, occurs in the temperature range 170-190 °C. This is irrespective of the pressure-velocity-power combinations. Similar results were found by Alemani et al.[25] when imposing different loading conditions at a fixed sliding velocity, for six different pad materials. However, it is interesting to note that all tested pad materials make use of phenolic resin as a binder that starts to transform for temperatures close to the transition one [35]. Therefore, an interesting hypothesis, also suggested by Kukutschova [10] is that phenolic resin could be the main element responsible for such high emissions, due to its transformation, degradation and burning.

According to the considered results, it is possible to indicate temperature as the main influencing factor for brake system emissions. However, this is a response parameter, directly related to the frictional power and the cooling capacity of the brake system. The controlled parameters, on the other hand, are not individually significant since they are susceptible to transition temperature effects.

Figure 6 maps  $k'_{\text{air}}$  coefficients, distinguishing between a coarse (6a,b), fine (6c,d) and ultrafine (6e,f) fraction. The presented results can be useful for simulation purposes [34] providing a specific particle coefficient based on fundamental system variables. If a static structural analysis provides the pressure distribution for each considered time step, together with the imposed sliding velocity, then the parameters to identify the proper  $k'_{\text{airFRACTION}}$  values are enabled. These, multiplied by their characteristic diameters (see Section 4), will give the overall emission for a specific moment.

Note that a limitation of the proposed method is that these diameters are susceptible to the selected measurement instrument and its resolution; this is because only the cut-off diameter of each stage is considered. Nevertheless, having particle coefficients that are specific to the size fraction helps reduce the calculation time while considering the possible changes in size distribution induced by different braking conditions.

Other than for simulations, these  $k'_{\text{air}}$  maps indicate that size fractions behave differently. The coarse and fine ones seem to be more sensitive to the sliding velocity whereas the ultrafine one seems to be

more sensitive to power and load. There are various reasons for this. First, bigger particles are highly influenced by gravitational and inertial forces. Therefore, increasing the system speed will enhance the kinetic energy of the particles. In addition, the flow turbulence will rise. All this leads to a longer stopping distance for the bigger particles [36], reducing the probability that they will settle before they reach the sampling point [37].

On the other hand, the ultrafine fraction appears more sensitive to frictional power and temperature, in accordance with previous literature [10,29,38] and the study results. Indeed, the  $k'_{\text{airULTRAFINE}}$  coefficients rise for increasing temperature values (see Figure 4), up to the maximum values shown for condition no.4. The only exception is test condition no.8. An explanation for such dependence of the ultrafine fraction is suggested from Namgung et al. [38], indicating evaporation taking place at the contact surface only for high temperature. Such phenomena would generate particles in the range of 20-40 nm where nucleation can take place increasing the particle number. In addition when concentrations are very high, agglomeration takes also place, generating particles in the range of 200 nm. Such indications are in a good relation with this paper results, both in terms of total concentration as well as in terms of  $k'_{\text{airULTRAFINE}}$  coefficient. However the latter cannot distinguish between different generation mechanisms, but can only provide indications on the overall probability that a particle in the ultrafine range can be produced.

An important limitation to this study is the absence of isokinetic sampling, causing particle losses. This does not affect the main outcomes of the study since all the tests were sampled using the same set-up. Nevertheless, when performing simulations, it is important to consider that  $k'_{\text{airCOARSE}}$  is affected by an error.

Future works should try to extend the testing conditions to get a more accurate mapping for higher energy, strengthening the results of this paper. A specific focus on phenolic resin would also be valuable in order to understand whether this is the real main contributor to emissions, especially for the ultrafine fraction.

## 7. CONCLUSIONS

A low-steel pad material was tested against a cast iron disc making use of a pin-on-disc tribometer specifically designed for particle measurements. Different nominal contact pressures and sliding velocities combinations were tested. The influence of the aforementioned parameters, the developed frictional power and the system temperature, on particle emissions was analysed. The results indicate that:

- System temperature is the most important factor affecting emissions due to the transition temperature which significantly affects the ultrafine levels. Transition temperature is not affected by the testing condition imposed here and lies in the range 170-190°C
- Among the typical brake system parameters, frictional power is the most important one. Similar frictional power can provide different outcomes regarding particle emissions in terms of total concentration, specific particle coefficient and size distribution, depending on the system temperature
- The specific particle coefficient for the ultrafine fraction is affected by frictional power and system temperature and increases as system temperatures rise

- The specific particle coefficient for the coarse and fine fraction is particularly affected by the sliding velocity and shows an increase when nominal contact pressure decreases

## ACKNOWLEDGEMENTS

This work was funded by the European Union Seventh Framework Programme (FP-PEOPLE-2012-IAPP) under the Rebrake Project (grant number 324385) and the European Union's Horizon 2020 research and innovation programme which is part of the LOWBRASYS Project (grant number 636592). The Authors would also like to thank Mr. Guido Perricone and Mr. Alessandro Ciotti at Brembo S.p.A. for their fundamental support to this research.

## REFERENCES

- [1] Grigoratos T, Martini G. Brake wear particle emissions: a review. *Environ Sci Pollut Res* 2015;22:2491–504. doi:10.1007/s11356-014-3696-8.
- [2] Hoffmann B, Moebus S, Möhlenkamp S, Stang A, Lehmann N, Dragano N, et al. Residential exposure to traffic is associated with coronary atherosclerosis. *Circulation* 2007;116:489–96. doi:10.1161/CIRCULATIONAHA.107.693622.
- [3] Gasser M, Riediker M, Mueller L, Perrenoud A, Blank F, Gehr P, et al. Toxic effects of brake wear particles on epithelial lung cells in vitro. *Part Fibre Toxicol* 2009;6:30. doi:10.1186/1743-8977-6-30.
- [4] Schwartz J, Laden F, Zanobetti A. The Concentration-Response Relation between PM<sub>2.5</sub> and Daily Deaths. *Environ Health Perspect* 2002;110:1025–9.
- [5] Lighty JS, Veranth JM, Sarofim a F. Combustion aerosols: factors governing their size and composition and implications to human health. *J Air Waste Manag Assoc* 2000;50:1565-1618-1622. doi:10.1080/10473289.2000.10464197.
- [6] Loomis D, Grosse Y, Lauby-Secretan B, Ghissassi F El, Bouvard V, Benbrahim-Tallaa L, et al. The carcinogenicity of outdoor air pollution. *Lancet Oncol* 2013;14:1262–3. doi:10.1016/S1470-2045(13)70487-X.
- [7] EEA. Air quality in Europe — 2014 report (EEA Technical Report No. 5/2014). 2014.
- [8] Wahlström J, Olofsson U. A field study of airborne particle emissions from automotive disc brakes. *Proc Inst Mech Eng Part D J Automob Eng* 2014;229:954407014550053. doi:10.1177/0954407014550053.
- [9] Sanders PG, Xu N, Dalka TM, Maricq MM. Airborne brake wear debris: Size distributions, composition, and a comparison of dynamometer and vehicle tests. *Environ Sci Technol* 2003;37:4060–9. doi:10.1021/es034145s.
- [10] Kukutschová J, Moravec P, Tomášek V, Matějka V, Smolík J, Schwarz J, et al. On airborne nano/micro-sized wear particles released from low-metallic automotive brakes. *Environ Pollut* 2011;159:998–1006. doi:10.1016/j.envpol.2010.11.036.
- [11] Garg B, Cadle S, Mulawa P, Groblicki P, Laroo C, Parr G. Brake wear particulate matter emissions, *Environ. Sci Technol* 2000;34:4463–9.
- [12] Wahlström J, Olander L, Olofsson U. Size, shape, and elemental composition of airborne wear particles from disc brake materials. *Tribol Lett* 2010;38:15–24. doi:10.1007/s11249-009-9564-x.
- [13] Mosleh M, Blau PJ, Dumitrescu D. Characteristics and morphology of wear particles from laboratory testing of disk brake materials. *Wear* 2004;256:1128–34.

- doi:10.1016/j.wear.2003.07.007.
- [14] Wahlström J, Gventsadze D, Olander L, Kutelia E, Gventsadze L, Tsurtsunia O, et al. A pin-on-disc investigation of novel nanoporous composite-based and conventional brake pad materials focussing on airborne wear particles. *Tribol Int* 2011;44:1838–43. doi:10.1016/j.triboint.2011.07.008.
- [15] Abbasi S, Jansson A, Olander L, Olofsson U, Sellgren U. A pin-on-disc study of the rate of airborne wear particle emissions from railway braking materials. *Wear* 2012;284–285:18–29. doi:10.1016/j.wear.2012.01.016.
- [16] Wahlström J, Söderberg a, Olander L, Olofsson U, Jansson a. Airborne wear particles from passenger car disc brakes: A comparison of measurements from field tests, a disc brake assembly test stand, and a pin-on-disc machine. *Proc Inst Mech Eng Part J J Eng Tribol* 2010;224:179–88. doi:10.1243/13506501JET633.
- [17] Metinoz I, Matejka V, Alemani M, Wahlström J, Perricone G. Could Pin-on-Disc Tribometers Be Used To Study the Friction/Wear Performance of Disc Brake Materials? *Eurobrake 2016 Conf Proc* 2016:1–10.
- [18] Wahlström J, Olander L, Olofsson U. A pin-on-disc study focusing on how different load levels affect the concentration and size distribution of airborne wear particles from the disc brake materials. *Tribol Lett* 2012;46:195–204. doi:10.1007/s11249-012-9944-5.
- [19] Wirth A, Eggleston D, Whitaker R. A fundamental tribochemical study of the third body layer formed during automotive friction braking. *Wear* 1994;179:75–81. doi:10.1016/0043-1648(94)90222-4.
- [20] Österle W, Griepentrog M, Gross T, Urban I. Chemical and microstructural changes induced by friction and wear of brakes. *Wear* 2001;251:1469–76. doi:10.1016/S0043-1648(01)00785-2.
- [21] Wahlström J, Söderberg A, Olofsson U. A cellular automaton approach to numerically simulate the contact situation in disc brakes. *Tribol Lett* 2011;42:253–62. doi:10.1007/s11249-011-9772-z.
- [22] Olofsson U, Olander L, Jansson A. A Study of Airborne Wear Particles Generated From a Sliding Contact. *J Tribol* 2009;131:44503. doi:10.1115/1.3176990.
- [23] Wahlström J, Olofsson U, Jansson A, Olander L. Airborne Wear Particles Emissions from Commercial Disc Brake Materials – Passenger Car Field Test 2008.
- [24] Perricone G, Wahlstro m J, Olofsson U. Towards a test stand for standardized measurements of the brake emissions. *Proc Inst Mech Eng Part D J Automob Eng* 2015. doi:10.1177/0954407015616025.
- [25] Alemani M, Nosko O, Metinoz I, Olofsson U. A study on emission of airborne wear particles from car brake friction pairs. *SAE Int J Mater Manuf* 2015;9:147–57. doi:10.4271/2015-01-2665.
- [26] Holmberg K, Andersson P, Erdemir A. Global energy consumption due to friction in passenger cars. *Tribol Int* 2012;47:221–34. doi:10.1016/j.triboint.2011.11.022.
- [27] Alemani M, Wahlström J, Matějka V, Metinoz I, Söderberg A, Perricone G, et al. On the scaling effects of measuring disc brake airborne particulate matter emissions – a comparison of a pin-on-disc inertia tribometer and an inertia dynamometer bench under dragging conditions. *Proc Inst Mech Eng Part J J Eng Tribol* 2017.
- [28] Montgomery DC. *Design and Analysis of Experiments*, 8th edition. 8th ed. 2012.
- [29] Alemani M, Olofsson U, Perricone G, Söderberg A, Wahlström J, Ciotti A. A Study on the Load Level Influence on Particulate Matter Emissions From the Sliding Contact Between a Low Steel Friction Material and Cast Iron. *Eurobrake 2015 Conf. Proc.*, Dresden: FISITA , May 2015; 2015.

- [30] Nosko O, Alemani M, Olofsson U. Temperature Effect on Emission of Airborne Wear Particles from Car Brakes. Eurobrake 2015 Conf. Proc., Dresden: FISITA , May 2015; 2015, p. EB2015-TEF-014.
- [31] Schauer JJ, Lough GC, Shafer MM, Park J-S. Characterization of Metals Emitted from Motor Vehicles. 2006.
- [32] Olofsson U, Olander L, Jansson A. Towards a model for the number of airborne particles generated from a sliding contact. *Wear* 2009;267:2252–6. doi:10.1016/j.wear.2009.05.002.
- [33] Archard JF, Hirst W. The Wear of Metals under Unlubricated Conditions. *Proc R Soc London Ser A, Math Phys Sci* 1956;236:397–410.
- [34] Wahlström J, Söderberg A, Olofsson U. Simulation of airborne wear particles from disc brakes. *SAE Tech. Pap.* 2009-01-3040, 2009. doi:10.4271/2009-01-3040.
- [35] Nam J, Seferis J, Yoon S. A viscoelastic study of glass transition and degradation process of phenolic resin/carbon fiber composite. *Korean J Rheol* 1999;11:9--17.
- [36] Hinds WC. *Aerosol Technology: properties, behavior, and measurement of airborne particles*. 2nd ed. Wiley-Interscience; 1999.
- [37] Liu H, Jonsson LTI, Jönsson PG. A simulation study of airborne wear particles from laboratory wheel-rail contacts. *Particuology* 2016;28:31–42. doi:10.1016/j.partic.2015.09.008.
- [38] Namgung HG, Kim JB, Woo SH, Park S, Kim M, Kim MS, et al. Generation of Nanoparticles from Friction between Railway Brake Disks and Pads. *Environ Sci Technol* 2016;50:3453–61. doi:10.1021/acs.est.5b06252.

## Research highlights

- ☒ System temperature is the most important factor affecting emissions due to the transition temperature which significantly affects the ultrafine levels. Transition temperature is not affected by the testing condition imposed here and lies in the range 170-190°C
- ☒ Among the typical brake system parameters, frictional power is the most important one. Similar frictional power can provide different outcomes regarding particle emissions in terms of total concentration, specific particle coefficient and size distribution, depending on the system temperature
- ☒ The specific particle coefficient for the ultrafine fraction is affected by frictional power and system temperature and increases as system temperatures rise
- ☒ The specific particle coefficient for the coarse and fine fraction is particularly affected by the sliding velocity and shows an increase when nominal contact pressure decreases